Journal of Materials Chemistry A

Accepted Manuscript

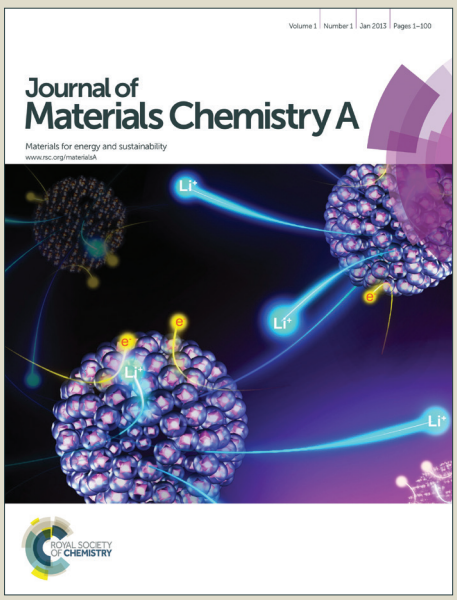

ROYAL SOCIETY OF CHEMISTRY

www.rsc.org/materialsA

Electrical characterization of $TiO_2/CH_3NH_3PbI_3$ heterojunction solar cells

Wenqiang Liu, Yang Zhang*

Institute for Physics of Microsystem, Key Laboratory of Photovoltaic Materials and Department of Physics, Henan University, Kaifeng, Henan 475004, China

ABSTRACT

$TiO_2/CH_3NH_3PbI_3$ heterojunction solar cells were fabricated by spin-coating and characterized with current-voltage, impedance spectroscopy and capacitance-voltage measurements. It was demonstrated that the $TiO_2/CH_3NH_3PbI_3$ layers form an ideal p-n heterojunction suitable for the photovoltaic application. The active acceptor concentration of 9.67×10^{15} cm^{-3} in $CH_3NH_3PbI_3$ layer and the built-in potential of 0.67 eV in $TiO_2/CH_3NH_3PbI_3$ heterojunction were derived by the Mott–Schottky relationship. Numerical simulation showed that the acceptor concentration in $CH_3NH_3PbI_3$ layer greatly influenced the electron potential barrier height at the junction interface. The degradation of $TiO_2/CH_3NH_3PbI_3$ heterojunction solar cells showed the efficiency remained 35.5% after storage under ambient laboratory conditions for 15 days. These results indicated that the oriented TiO_2 layers provide a possible route to fabricate stable perovskite-based photovoltaic devices without hole transporting materials.

Keywords: Lead halide perovskites; Solar cells; Heterojunction Impedance spectroscopy; Capacitance-voltage

*Corresponding author: Y. Zhang, email: yzhang@henu.edu.cn

1. Introduction

Recently, methylammonium lead halide perovskite-based solar cells have attracted considerable attention as candidates for the next generation of low-cost and high-performance photovoltaic devices.[1-5] Organometal halide perovskites, $CH_3NH_3PbI_3$ and $CH_3NH_3PbCl_3$, have been proven key materials in the fabrication of high efficiency perovskite solar cells.[6,7] In the past two years, remarkable progress has been made in power conversion efficiency (PCE) by rational design of structures and control of interfaces.[8-10] Their PCEs have achieved over 15%.[11] Usually, such devices have two different configurations: the hole-transporting material infiltrated mesoporous TiO_2 nanostructures,[12,13] and a simple planar heterojunction.[14] In mesoporous nanostructured devices, the function of organometal halide perovskites is usually regarded as a sensitizer. Mesoporous films are infiltrated with organometal halide perovskite and Hole-Transporting Materials (HTM) extract holes from the light absorption layer of organometal halide perovskite.[15] On the other hand, n-type metal oxides as an electron transporter combine with organometal halide perovskites to form a p-n junction without additional HTMs. Organometal halide perovskites are used as an efficient light absorber and HTM simultaneously. Apparently, such photovoltaic devices without HTM are simpler, and save the cost of raw materials. Recently, Lioz Egar first fabricated hole-conductor-free heterojunction solar cells based on $CH_3NH_3PbI_3$ pervoskite, which acted as an absorber and HTM at the same time.[16] Although the performance of such solar cells is still needed to be enhanced, they have great potential in real applications. However, the mechanism of electron

transport in the interface of p-n junction based on perovskite is not completely clear. Therefore, it is important to investigate the electrical properties of the p-n junction interface in the pervoskite-based solar cells without HTMs.

In this work, $CH_3NH_3PbI_3$ was deposited on the oriented TiO_2 grown in an ethanol–solvothermal system by a spin-coating method. The electrical properties of TiO_2 and $CH_3NH_3PbI_3$ interface were investigated by impedance spectroscopy, capacitance-voltage (*C-V*) measurements.

2 Experimental

2.1 Materials synthesis

Methylammonium iodide (CH_3NH_3I) was synthesized and purified using a modified process based on a previously reported method.[17] 10 mL of hydroiodic acid (57 wt.%, Tianjin Kemiou Co. Ltd.) and 14 mL of methylamine (40% in methanol, Tianjin Kemiou Co. Ltd.) were stirred in the ice bath for 2 h. The resulting solution was evaporated at 90 ^{o}C. The yellowish raw product was obtained and finally recrystallized with methanol washing five times. The obtained product (CH_3NH_3I) was dried at 60 °C in a vacuum oven for 24 h. The perovskite precursor solution was prepared by mixing the as-synthesized CH_3NH_3I and lead (II) iodide (PbI_2) with a mole ratio of 1:1 in N,N-Dimethylformamide (DMF) at 60 °C for 12 h.

FTO-coated glass (14 ohm/sq, Nippon Sheet Glass, Japan) was cleaned by sonication in detergent, acetone, 2-propanol, and ethanol. After cleaning, a TiO_2 layer was deposited by spin-coating at 2000 rpm, heated at 450 ^{o}C for 30 min in air. TiO_2 colloid solution was prepared following the procedure reported previously.[18] Briefly,

tetra-n-butyl-titanate (1 mL) was dropped into ethanol (6 mL) under stirring for 60 min. Acetylacetone (1 mL) was added with stirring 40 min, ethanol (3 mL) was added. Then, acetic acid (1 mL) solutions were added into the solution, stirred for 30 min, subsequently spun coating at 2000 rpm for 40 s.

The oriented TiO_2 films on compact TiO_2 coated FTO substrates were synthesized by an ethanol–HCl solvothermal process following a similar procedure reported previously.[19] In a typical process, 0.7 ml tetrabutyl titanate was added into a mixture of 20 mL of absolute ethanol and 20 ml 37 wt % HCl. After stirring, the mixture was transferred to a Teflon-lined stainless steel autoclave (100 mL). Four substrates were placed in the same autoclave with the conducting side facing the wall of autoclave. The solvothermal reaction was carried out at 170 °C for 1 h in a vacuum oven. Then, the autoclave was cooled to room temperature naturally. The samples were rinsed with ethanol and deionized water. After dried in air, they were heated in a furnace at 450 ^{o}C and maintained for 1 h, subsequently raised to 550 ^{o}C and maintained for 1 h.

2.2 Solar cell fabrication

The above perovskite precursor solution was spread on the annealed TiO_2 films and spun at 2000 rpm for 40 s followed in an argon-filled glove box. Then the films were heated at 120 °C for 30 min. Finally, a gold film (~220 nm) was deposited on the top of perovskite layer by thermal evaporation at a pressure of 10^{-3} Pa to complete the cell device. The active area of ~0.08 cm^2 for the devices was determined by a shadow mask.

2.3 Characterization

The cross-sectional structure of the solar cells was examined by a scanning electron microscope (SEM) (JEOL, JSM-7001F, JEOL). The current density–voltage (*J-V*) characteristics were measured using a Keithley 2440 Sourcemeter in air under AM 1.5 G illumination from a Newport Oriel Solar Simulator with an intensity of 100 mW/cm^2. The electrochemical impedance measurements were carried out under forward bias of 0.68 V in the dark using an electrochemical workstation (RST5200, Zhengzhou Shiruisi Instrument Co., Ltd.) with the frequency range from 10 Hz to 139 kHz. The magnitude of the alternative signal was 10 mV. Capacitance-voltage measurements were performed at fixed frequencies of 2 kHz, 8 kHz and 20 kHz in the dark, respectively. All measurements were carried out in air at room temperature.

3. Results and discussion

3.1. Cross-sectional SEM image of the device

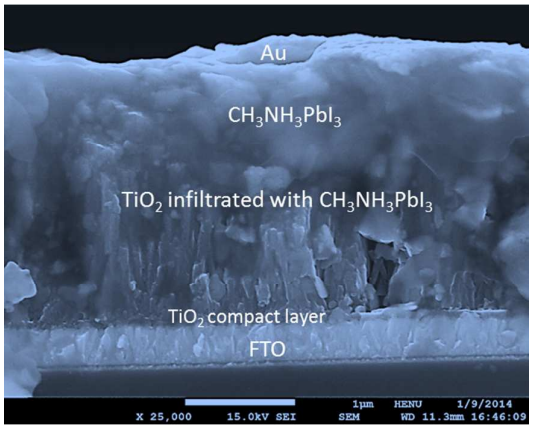

Figure 1. Cross-sectional SEM image of the device based on $CH_3NH_3PbI_3$ and oriented TiO_2 film prepared by a solvothermal process.

Figure 1 shows a cross-sectional SEM image of the device based on

$CH_3NH_3PbI_3$ and oriented TiO_2 film prepared by an ethanol-HCl solvothermal process. X-ray diffraction (XRD) characterization shows that the intensity of the (002) peak of rutile TiO_2 is the strongest in all peaks (Supporting Information, Figure S1), indicating that the growth of TiO_2 is highly oriented along the (002) plane on FTO substrate during the solvothermal reaction process. This result is in good agreement with the oriented TiO_2 film observed by the cross-sectional SEM image in Figure 1. The thicknesses of the Au layer, oriented TiO_2, compact TiO_2 film can be evaluated to be 220 nm, 2.5 μm, and 30 nm, respectively. TiO_2 film prepared by a solvothermal process shows the oriented rod-type TiO_2 structure, indicating that TiO_2 was densely formed on the compact TiO_2 film. $CH_3NH_3PbI_3$ perovskite was infiltrated into the oriented TiO_2. Previous studies have demonstrated that electron transport in one-dimensional structures is intrinsically faster than that in mesoporous TiO_2 nanoparticle films.[20,21] Also, it should be noted that the $CH_3NH_3PbI_3$ did not form a continuous phase, which indicated that it had infiltrated to the upper part of the oriented TiO_2 film, but had not infiltrated to its bottom. This case is different from the previously reported porous TiO_2 film with full infiltration of perovskite.[17,22]

3.2. Current density-voltage (*J-V*) characteristics

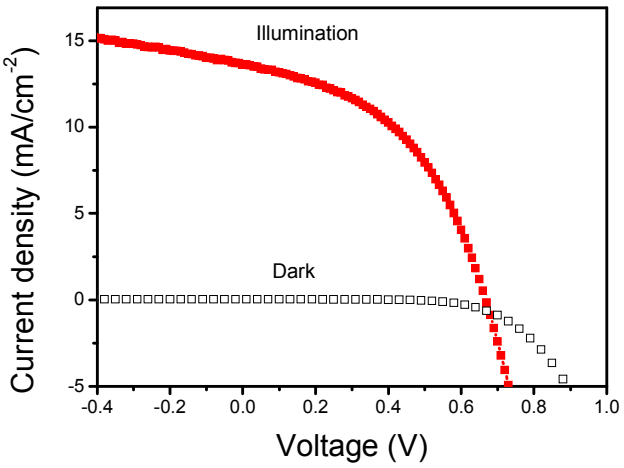

Figure 2. *J–V* characteristics of the $CH_3NH_3PbI_3/TiO_2$ heterojunction solar cell in the dark (open symbols) and under illumination (solid symbols) of 100 mW/cm^{-2}.

Figure 2 shows the *J–V* characteristics of the heterojunction device consisting of FTO, compact TiO_2, oriented-TiO_2, $CH_3NH_3PbI_3$ perovskite and Au in the dark (open symbols) and under illumination (solid symbols) of AM 1.5G simulated solar spectrum. Positive bias is defined as positive voltage applied to the Au electrode. The clear rectifying behavior can be observed with and without illumination. A high rectification ratio of ~ 500 from the device is obtained in the dark. Under illumination, the solar cell exhibits the short circuit current density (J_{sc}) of 13.6 mA/cm^2; open circuit voltage (V_{oc}) of 0.67 V; fill factor (FF) of 45.8% and PCE of 4.2%. On the other hand, as we can see there is much difference in *J-V* curves near the open-circuit voltage under illumination and in the dark. The exact origin of this behavior is unclear at present. However, this result is in good agreement with previously reported results of other kinds of solar cells.[23,24]

3.3. Impedance spectra of $TiO_2/CH_3NH_3PbI_3$ solar cells

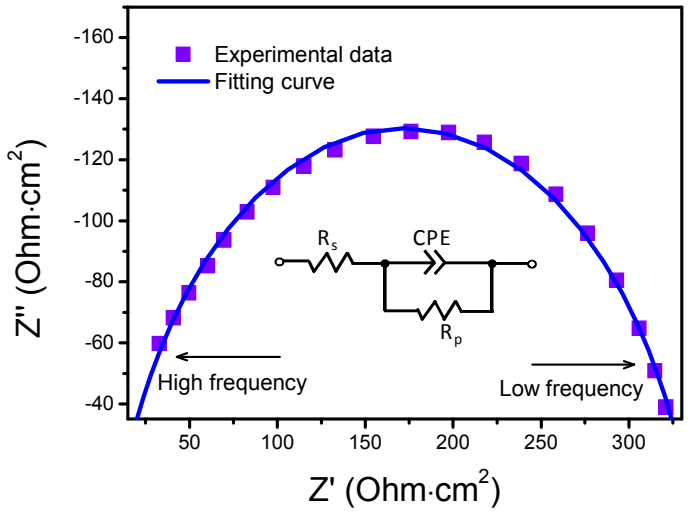

Figure 3. Typical Nyquist plot of a solar cell based on TiO_2/$CH_3NH_3PbI_3$ in the dark. The simulation result (solid line) is fitted to experimental data (symbols) using the equivalent circuit for fitting in the insert.

To analyze the interfacial recombination at the interface between the TiO_2 and $CH_3NH_3PbI_3$, impedance spectroscopy measurements were carried out in the dark. Figure 3 shows the Nyquist plots of the TiO_2/$CH_3NH_3PbI_3$ heterojunction solar cell in the dark. The equivalent circuit in the inset of Figure 3 is used to fit the experimental data (symbols). DC voltage of 0.7 (near the Voc of the solar cell) was applied during the measurement and 10 mV AC signals were applied for a frequency range from 10 Hz to 139 kHz. When the impedance measurements are performed under the V_{oc}, the modulated small-amplitude voltage U_{AC} is superimposed to the V_{oc}. At this bias voltage, the solar cell is almost in operation under actual conditions. In Figure 3, there is only one semicircle attributed to the electron transfer process at the TiO_2 and $CH_3NH_3PbI_3$ interface, implying that there is only one junction in the

$TiO_2/CH_3NH_3PbI_3$ heterojunction solar cell. It is different from the previous reported two semicircles in the perovskite-sensitized solar cells with spiro-MeOTAD HTM.[13] The absence of another semicircle is likely due to the absence of HTM in this device structure. The single semicircle also indicates that the interface contacts between $CH_3NH_3PbI_3$ and TiO_2. This is due to the contacts between Au and $CH_3NH_3PbI_3$ or FTO and TiO_2 are Ohmic contacts, rather than the rectifying contact. Because the work function (-5.1 eV) of the metal Au is higher than the highest occupied molecular orbital (-5.43 eV) (the top of valence band), this difference can lead to hole diffusion from $CH_3NH_3PbI_3$ to Au. In the case of an Ohmic contact, there are no interfaces related to charging and discharging. Therefore, the semicircle was attributed to the $TiO_2/CH_3NH_3PbI_3$ heterojunction interface. The fitting curve by the equivalent circuit model shown in the inset of Figure 3 is in good agreement with experimental data. It indicates that the electron elements in the circuit model can represent the real functional components. The equivalent circuit consists of a series resistor (R_s) and two parallel combinations of a resistor (R_p) and a constant phase element (CPE). The fitted value of R_s, representing the Ohmic resistance in the device, is 7.7 Ω cm^2. R_p is associated with the interface charge transport process, defined by the charge transfer resistance, and CPE suggests a non-ideal behavior of the capacitor. It is usually defined by two values, CPE-T and CPE-P. If CPE-P equals 1, then the CPE is identical to an ideal capacitor without defects and/or grain boundary.[25,26] The fitting of the present data shows that the value of CPE-P is 0.853. This indicates that the interface capacitance between oriented TiO_2 and $CH_3NH_3PbI_3$ is not perfect

electrically, which is due to an inhomogenous manner of rough interface. The fitted value of R_p is 329 Ω cm^2, resulting from the charge transport across the $TiO_2/CH_3NH_3PbI_3$ heterojunction.

3.4. *C-V* characteristics of a typical device

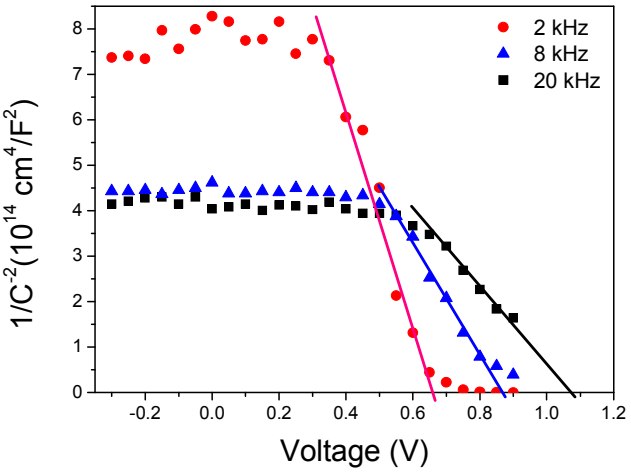

Figure 4. Mott-Schottky plots for the $TiO_2/CH_3NH_3PbI_3$ heterojunction solar cell at 2 kHz, 8 kHz, 20 kHz in the dark. The solid lines are linear fits to the experimental data.

Generally, *C-V* measurements can provide important information on the nature of the semiconductor interface and charge transport. *C-V* characteristics of a typical device based on the $CH_3NH_3PbI_3/TiO_2$ heterojunction have been measured at various frequencies in the dark at room temperature. Figure 4 shows the Mott-Schottky plots at various frequencies. The solid lines are linear fits to the experimental data. The good agreement between the linear fits and the experimental data indicate a uniformly charge distribution region for the device. The built-in potential (V_{bi}) of semiconductor p-n junction can be estimated from the Mott-Schottky equation[27]

$$\frac{1}{C_s^2} = \frac{2}{q\varepsilon\varepsilon_0 N}(V - V_{bi} - kT/q) \quad (1)$$

where C_s is the space charge capacitance per unit area, and q, ε, ε_0 are the charge of electron, the dielectric constant of the semiconductor, the permittivity of free space, respectively. N, V, V_{bi}, k and T are the carrier density, the applied bias voltage, the built-in potential, Boltzmann constant and absolute temperature, respectively. At room temperature kT/q in Eq. 1 is 0.026 V. Figure 4 shows the Mott-Schottky plots at different frequencies. In the high (0 to 1.0 V) forward bias region the C_s^{-2} vs V plots are linear for different frequencies. This linearity implies the formation of a barrier between TiO_2/ $CH_3NH_3PbI_3$ p-n junction. The intercepts of the straight lines yield 0.67 V, 0.86 V, and 1.13 V at 2 kHz, 8 kHz, 20 kHz, respectively. Apparently, these plots show the dependence of frequency dispersion. That is, the capacitance decreased with increasing frequency. This indicates a contribution to the junction space charge from relatively slow deep levels at or near the interface of $CH_3NH_3PbI_3/TiO_2$. This result is in agreement with the above inhomogenous interface obtained by impedance analysis. According to the dielectric constant of 6.5 determined by the diffuse reflection of the $CH_3NH_3PbI_3$ powder,[28] active hole concentrations (N_A) are derived to be 9.67×10^{15} cm^{-3}, 1.7×10^{16} cm^{-3}, and 3.1×10^{16} cm^{-3} by the slopes of the lines at frequencies of 2 kHz, 8 kHz, and 20 kHz, respectively. Standard p-n junction solar cell theory predicts that the V_{oc} of the device under illumination is closely related to the V_{bi} of junction.[29] Therefore, The value of V_{bi} (0.67 V) obtained at 2 kHz is in good agreement with the previous reported,[30] and close to the V_{oc} of the device under 1-Sun illumination (100 mW/cm^2), obtained from the *J-V* curve shown in Figure 2. While, the values (0.86, 1.13 V) obtained at 8 kHz and 20 kHz are larger than V_{oc} of the solar

cell. This may be attributed to the presence of surface states was usually considered to contribute the continuous film capacitance.[31] Surface states may be due to an inhomogeneous distribution of crystal sizes at the film surface or interface. At higher frequencies carrier diffusion at surface is not able to follow the ac signal. This random motion does not yield a net motion of carriers nor yield a net current in material with a uniform carrier density as any carrier which leaves a specific location is on average replace by another one. Therefore, the active acceptor concentration N_A on the more lowly doped side of the junction determined by plotting $1/C^2$ vs V at high frequencies is higher than at low frequencies. The intercept with the voltage axis gives the larger V_{bi} than obtained at low frequencies.

3.5. The simulated energy band diagram

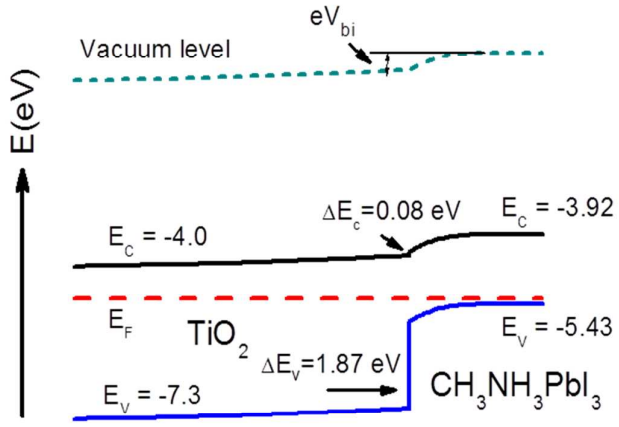

Figure 5. The simulated energy band diagram for the $TiO_2/CH_3NH_3PbI_3$ heterojunction solar cell with the active acceptor concentration of 9.67×10^{15} cm^{-3} at the thermal dynamic equilibrium condition.

To understand the energy band structure, the band diagram in the dark for the $TiO_2/CH_3NH_3PbI_3$ heterojunction was simulated according to N_A of 9.67×10^{15} cm^{-3} obtained by *C-V* characteristics, the electron affinity of 3.92 eV and energy gap of 1.51 eV of $CH_3NH_3PbI_3$,[32] using the AMPS-1D software (Analysis of Microelectronic and Photonic Structures).[33] A TiO_2 layer with a band gap of 3.3 eV is used as the transparent window for the solar spectrum to be harvested by the $CH_3NH_3PbI_3$ layer. Figure 5 shows the simulated energy band diagram for the $TiO_2/CH_3NH_3PbI_3$ heterojunction solar cell at the thermal dynamic equilibrium condition. The inclined band diagram of the $CH_3NH_3PbI_3$ layer indicates a good potential profile in the depletion region for effective carrier separation. The interface valence and conduction band discontinuities (ΔEv=0.08 eV and ΔEc=1.87 eV) are observed. The large ΔEv at the n-layer side seen in the band diagram hinders the hole flowing from p-layer side $CH_3NH_3PbI_3$ layer to n-TiO_2 layer. The barrier at p-side resists the electron diffusion from n-type TiO_2 side to p-type $CH_3NH_3PbI_3$ side. This can improve carrier collection. It is also found that $CH_3NH_3PbI_3$ can overwhelmingly contribute to the built in potential barrier (eV_{bi}). The large values of eV_{bi} and ΔEv can lead to large J_{sc} and V_{oc} of such devices based on the $TiO_2/CH_3NH_3PbI_3$ heterojunction. Thus, the combination TiO_2 and $CH_3NH_3PbI_3$ layers formed an ideal p-n heterojunction suitable for the photovoltaic application.

3.6. The air-stability of the$TiO_2/CH_3NH_3PbI_3$ heterojunction solar cell

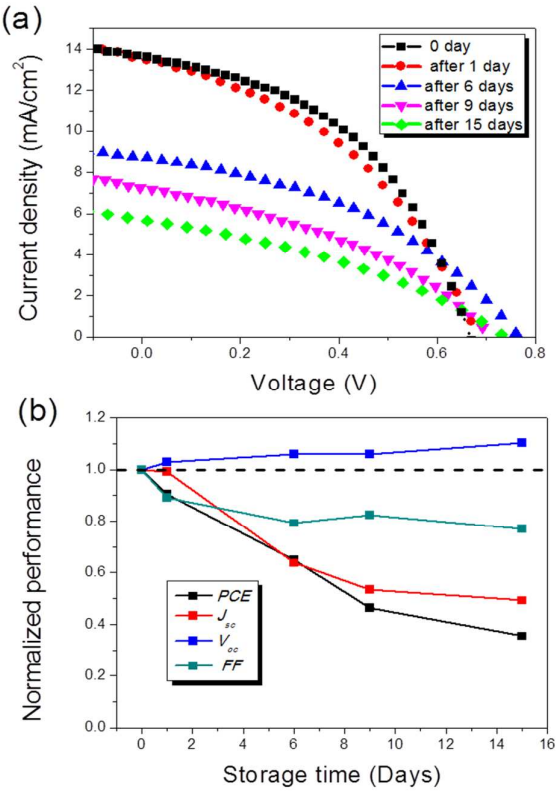

Figure 6. (a) *J-V* characteristics of the $TiO_2/CH_3NH_3PbI_3$ heterojunction solar cell without encapsulation over a period of 15 days in air under ambient conditions. (b) Normalized performance parameters as a function of storage time for the device based on $TiO_2/CH_3NH_3PbI_3$ heterojunction solar cell exposed to ambient air for 15 days without encapsulation.

As we all know, perovskite-type hybrids are easily degraded in the presence of moisture due to the hygroscopic amine salts. Thus, there is very little published research on the topic. These solar cells usually exhibit serious degradation of PCE after exposure to humidity air for few days.[34] However, the stability of solar cells is very important to commercialized application. So, the air stability of the $TiO_2/CH_3NH_3PbI_3$ heterojunction solar cell was also investigated. The typical device

without encapsulation was stored under ambient conditions and periodically tested for 15 days to gauge the device stability. The air stability properties of devices based on $TiO_2/CH_3NH_3PbI_3$ heterojunction as a function of storage time in air under ambient conditions is shown in Figure 6 (a). All the photovoltaic performance parameters were normalized to their original values, and plotted in Figure 6 (b). It can be seen that the PCE degradation occurred gradually. After exposed to the laboratory air ambient for 9 days and 15 days, the PCEs decreased about 53.6% and 64.5% of the original value. According to our experiences, the performance of solar cells based on lead iodide perovskite sensitized porous TiO_2 degraded rapidly. It was even disappeared completely in few minutes. So, this device is much more stable than the conventional device based on lead iodide perovskite sensitized porous TiO_2. It should be noted that the V_{oc} increased with storage time as shown in Figure 6 (b). This may be attributed to the increase of resistance in cell, which is confirmed by Nyquist plots of the freshly prepared cell and its degraded cell stored 15 days in air ambient (Supporting Information, Figure S2). Generally, the V_{oc} would be increased due to the increase of R_s. On the other hand, R_p is dominated by the interface charge transport process. Larger R_p represents less recombination in charge transport process, which can lead to improved collection of charge carriers at open circuit. Thus higher V_{oc} value can be obtained. However, increasing with the resistance, the photocurrents and fill factor may be reduced, as shown in Figure 6 (a). The downtrend of J_{sc} and PCE indicates that degradation of PCE is mainly caused by the decrease of J_{sc}. However, J_{sc} goes down rapidly with increasing storage time, which is attributed to the increase of series

resistance in device. The degradation can be attributed to the reaction of $CH_3NH_3PbI_3$ perovskites with oxygen or water in air. The relative stability of this device may be due to the compact and oriented TiO_2 film, which prevented the over infiltration of perovskites. Therefore, the selection of the oriented TiO_2 film plays a role in the improved device stability.

4. Conclusions

The heterojunction solar cells based on $CH_3NH_3PbI_3$ and TiO_2 film grown in an ethanol–HCl solvothermal system were fabricated. Impedance spectroscopy and *C-V* measurements demonstrated that the combination of $CH_3NH_3PbI_3$ and TiO_2 formed an ideal p-n heterojunction. The active hole concentration in p-$CH_3NH_3PbI_3$ and the built-in potential of TiO_2/$CH_3NH_3PbI_3$ were derived by the Mott–Schottky relationship. According to the obtained data, a schematic energy-level diagram for TiO_2/$CH_3NH_3PbI_3$ heterojunction at the thermal dynamic equilibrium condition was given by numerical simulation. It was found that $CH_3NH_3PbI_3$ can overwhelmingly contribute to the electron potential barrier. The high active hole concentration is desired to improve the performance of $CH_3NH_3PbI_3$ based photovoltaic devices. The high efficiency of such devices based on the TiO_2/$CH_3NH_3PbI_3$ heterojunction is attributed to the large values of eV_{bi} and ΔEv. The degradation behavior of TiO_2/$CH_3NH_3PbI_3$ heterojunction solar cells without encapsulation showed that PCE remained 35.5% after storage under ambient laboratory conditions for 15 days. Therefore, the combination of the oriented TiO_2 layer and $CH_3NH_3PbI_3$ formed an ideal p-n heterojunction suitable for the photovoltaic application. Moreover, the

compact and oriented TiO_2 layers may play a crucial role in the stability of such solar cells.

Acknowledgments

This work was supported by the Department of Education, Henan Province under contract No. 13A480062.

References

1 J. Burschka, N. Pellet, S.J. Moon, R.H. Baker, P. Gao, M.K. Nazeeruddin and M. Grätzel, *Nature*, 2013, 499, 316–319.

2 H.J. Snaith, *J. Phys. Chem. Lett.*, 2013, 4, 3623–3630.

3 O. Malinkiewicz, A. Yella, Y.H. Lee, G.M. Espallargas, M. Grätzel, M.K. Nazeeruddin and H.J. Bolink, *Nat. Photonics,* 2014, 8, 128–132.

4 N.G. Park, *J. Phys. Chem. Lett.*, 2013, 4, 2423–2429.

5 H.S. Kim, S.H. Im and N.G. Park, *J. Phys. Chem. C*, 2014, 118, 5615–5625.

6 P.P. Boix, K. Nonomura, N. Mathews and S.G. Mhaisalkar, *Mate. Today*, 2014, 17, 16–23.

7 G. Hodes and D. Cahen, Nat. Photonics, 2014, 8, 87–88.

8 J.M. Ball, M.M. Lee, A. Hey and H.J. Snaith, *Energy Environ. Sci.*, 2013, 6, 1739-1743.

9 M. He, D. Zheng, M. Wang, C. Lin and Z. Lin, *J. Mater. Chem. A*, 2014, 2, 5994-6003.

10 D.Y. Liu and T.L. Kelly, *Nat. Photonics*, 2014, 8, 133–138.

11 M. Liu, M.B. Johnston and H.J. Snaith, *Nature*, 2013, 501, 395–398.

12 E.J.W. Crossland, N. Noel, V. Sivaram, T. Leijtens, J.A.A. Webber and H.J. Snaith, *Nature*, 2013, 495, 215–219.

13 H.S. Kim, J.W. Lee, N. Yantara, P.P. Boix, S.A. Kulkarni, S. Mhaisalkar, M.

Grätzel and N.Gyu. Park, *Nano Lett.*, 2013, 13, 2412−2417.

14 G.E. Eperon, V.M. Burlakov, P. Docampo, A. Goriely and H.J. Snaith, *Adv. Funct. Mater.,* 2014, 24, 151–157.

15 T. Leijtens, G.E. Eperon, S. Pathak, A. Abate, M.M. Lee and H.J. Snaith, *Nat. Commun.*, 2013, 4, 2885.

16 L. Etgar, P. Gao, Z. Xue, Q. Peng, A.K. Chandiran, B. Liu, Md. K. Nazeeruddin, and M. Grätzel, *J. Am. Chem. Soc.*, 2012, 134, 17396–17399.

17 H.S. Kim, C.R. Lee, J.H. Im, K.B. Lee, T. Moehl, A. Marchioro, S.J. Moon, R.H. Baker, J.H. Yum, J.E. Moser, M.Grätzel and N.G. Park, *Sci. Rep.-UK*, 2012, 2, 591.

18 S.S. Yuan,Y. Zhang, W.Q. Liu and W.F. Zhang, *Electrochim. Acta,* 2014, 116, 442–446.

19 X.J. Feng, K. Zhu, A.J. Frank, C.A. Grimes and T.E. Mallouk, *Angew. Chem. Int. Ed,* 2012, 51, 2727–2730.

20 B. H. Lee, M. Y. Song, S. Y. Jang, S. M. Jo, S. Y. Kwak and D. Y. Kim, *J. Phys. Chem. C*, 2009, 113, 21453–21457;

21 K. Zhu, N. R. Neale, A. Miedaner and A. J. Frank, *Nano Lett.*, 2007, 7, 69– 74.

22 U. Rammelt and G. Reinhard, *Electrochim. Acta,*1990, 35, 1045–1049.

23 W.J. E. Beek, M.M. Wienk and R.A.J. Janssen, *Adv. Funct. Mater.*, 2006, 16, 1112-1116.

24 M. Glatthaar, M. Riede, N. Keegan, K. Sylvester-Hvid, B. Zimmermann, M. Niggemann, A. Hinsch and A. Gombert, *Sol. Energ. Mat. Sol. C.*,2007, 91, 390–393.

25 G. Perrier, R. Bettignies, S.Berson, N. Lemaître and S. Guillerez, *Sol. Energ. Mat. Sol. C.*, 2012, 101, 210–216.

26 J.B. Jorcin, M.E. Orazem, N. Pébère and B. Tribollet, *Electrochim. Acta*, 2006, 51,

1473–1479.

27 R. van de Krol, A. Goossens and J. Schoonman, *J. Electrochem. Soc.*, 1997, 144, 1723-1727.

28 M. Hirasawa, T. Ishihara, T. Goto, K. Uchida and N. Miura, *Physica B*, 1994, 201, 427–430.

29 A. Straub, R. Gebs, H. Habenicht, S. Trunk, R. A. Bardos, A. B. Sproul and A.G. Aberle, *J. Appl. Phys.,* 2005*,* 97, 083703.

30 W.A. Laban and L. Etgar, *Energy Environ.Sci*, 2013, 6, 3249-3253.

31 S. Kapusta and N. Hackerman, *Eletrochim. Acta*, 1980, 25, 949-955.

32 Y.S. Kwon, J. Lim, H.J. Yun, Y.H. Kim and T. Park, *Energy Environ. Sci.*, 2014, 7, 1454-1460.

33 See http://www.ampsmodeling.org/, where one can download software AMPS (Analysis of Microelectronic and Photonic Structures), developed at Pennsylvania State University by the group of Prof. S. Fonash.

34 J.H. Noh, S.H. Im, J.H. Heo, T.N. Mandal and S. Seok, *Nano Lett.*, 2013, 13, 1764–1769.

Graphical abstract

Electrical properties of $TiO_2/CH_3NH_3PbI_3$ heterojunction